J. Fluid Mech. (2008), *vol.* 595, *pp.* 323–339.
doi:10.1017/S0022112007009305 Printed in the United Kingdom

Flow in a commercial steel pipe

L. I. LANGELANDSVIK[1], G. J. KUNKEL[2] AND A. J. SMITS[2]

[1]Department of Energy and Process Engineering,
Norwegian University of Science and Technology, N-7491 Trondheim, Norway
[2]Department of Mechanical and Aerospace Engineering,
Princeton University, Princeton NJ 08540, USA

(Received 5 February 2007 and in revised form 17 September 2007)

Mean flow measurements are obtained in a commercial steel pipe with $k_{rms}/D = 1/26\,000$, where k_{rms} is the roughness height and D the pipe diameter, covering the smooth, transitionally rough, and fully rough regimes. The results indicate a transition from smooth to rough flow that is much more abrupt than the Colebrook transitional roughness function suggests. The equivalent sandgrain roughness was found to be 1.6 times the r.m.s. roughness height, in sharp contrast to the value of 3.0 to 5.0 that is commonly used. The difference amounts to a reduction in pressure drop for a given flow rate of at least 13 % in the fully rough regime. The mean velocity profiles support Townsend's similarity hypothesis for flow over rough surfaces.

1. Introduction

Here we report flow measurements in a commercial steel pipe covering the smooth, transitionally rough, and fully rough regimes. This is the second of our investigations of rough pipe flow, the first being that by Shockling, Allen & Smits (2006), who studied the flow in a pipe with a honed surface, which is typical of many engineering applications. In the study reported here, the Reynolds number was varied from 150×10^3 to 20×10^6, with $k_{rms}/D = 1/26\,000 = 38.5 \times 10^{-6}$, where k_{rms} is the r.m.s. roughness height and D is the pipe diameter. As far as the authors are aware, the only other study of flow in a commercial steel pipe was performed by Bauer & Galavics (1936) and Galavics (1939), and we will demonstrate that the surface finish of their pipes is considerably different from that seen in a modern commercial steel pipe.

Despite the importance of 'natural' roughness in engineering applications, laboratory studies have typically focused on geometric roughnesses, such as square bars and meshes, or other artificial surfaces such as sandpaper. The most complete data set on rough pipe flow behaviour is still that obtained by Nikuradse (1933) using sandgrain roughness. As a result, the roughness of other surfaces is often expressed in terms of an 'equivalent sandgrain roughness', k_s, where k_s is found by comparing the friction factor of the surface in the fully rough regime to the friction factor of the equivalent sandgrain roughened pipe. For example, the Moody diagram (Moody 1944) uses k_s to describe the friction factor curves for rough pipes, and to find the friction factor for a given surface finish the equivalent sandgrain roughness must first be specified, which at present can only be found empirically.

Many aspects of the Moody diagram are currently being re-examined. For turbulent flow in the smooth regime, it uses the Blasius (1913) and Prandtl (1935) friction factor correlations. McKeon, Zagarola & Smits (2005) recently showed that Prandtl's friction

factor correlation is inaccurate at higher Reynolds numbers, and they proposed that for $Re_D \geqslant 300 \times 10^3$, a better correlation was given by

$$\frac{1}{\sqrt{\lambda}} = 1.930 \log Re_D \lambda - 0.537, \tag{1.1}$$

where Re_D is the Reynolds number based on the diameter and the bulk velocity $\overline{U}$, ρ is the fluid density and λ is the friction factor defined by

$$\lambda = \frac{-\mathrm{d}p/\mathrm{d}x}{\frac{1}{2}\rho \overline{U}^2} D \tag{1.2}$$

where $\mathrm{d}p/\mathrm{d}x$ is the streamwise pressure gradient. Equation (1.1) gives higher friction factors than the Prandtl formulation for $Re_D > 3 \times 10^6$ (up to 3.2 % higher at 10^8).

In the transitionally rough regime, the Moody diagram uses the Colebrook (1939) correlation, given by

$$\frac{1}{\sqrt{\lambda}} = -2 \ln \left(\frac{k_s}{3.71 D} + \frac{2.51}{Re_D \sqrt{\lambda}} \right). \tag{1.3}$$

This correlation is based on laboratory experiments on rough pipes performed by Colebrook & White (1937), as well as a large collection of friction factor data obtained from pipes in commercial use. Its form was constructed by asymptotically matching Prandtl's friction factor curve at low Reynolds number, and Nikuradse's fully rough, Reynolds-number-independent region at high Reynolds numbers. It is clear that the correlation does not describe well many rough surfaces, including the surfaces studied by Colebrook & White (1937). In particular, the correlation fails to reproduce the inflectional characteristics of sandgrain roughness, where the friction factor departs from the smooth correlation at some low value, and then increases in value before reaching its asymptotic high-Reynolds-number level in the fully rough regime. Hama (1954) studied a wide range of roughness types, including meshes and sandpaper roughnesses, and found that instead of following the Colebrook transitional roughness function they all displayed an inflectional behaviour in the transitionally rough regime. Furthermore, the departure from the smooth curve was often abrupt, rather than slowly varying, as implied by the Colebrook correlation.

This inflectional behaviour was also seen by Shockling *et al.* (2006) in a study of honed surface roughness. These results contradict the suggestion by Bradshaw (2000) that the abrupt or inflectional behaviour is only seen in an artificially roughened surface, and that the transition will resemble the Colebrook (1939) correlation (equation (1.3)) for natural surfaces. The equivalent sandgrain roughness of the surface was found to be $k_s \simeq 3\, k_{rms}$, in agreement with the suggestions of Zagarola & Smits (1998) for a surface produced by a similar honing process. The flow showed the first symptoms of roughness when $k_s^+ \approx 3.5$, contrary to the value implied by the Moody diagram, and the departure was much more abrupt than implied by the Colebrook correlation assumed by Perry, Hafez & Chong (2001). Finally, the large-diameter natural gas transmission pipelines on the Norwegian Continental Shelf have a surface finish similar to a honed finish, and Langelandsvik *et al.* (2005) found that operational data support a variant of the abrupt behaviour, although none of the data sets cover a large enough range of Reynolds numbers to fully determine the shape of the curve in the transitionally rough regime.

The scaling of the mean velocity U in a rough pipe was discussed by Shockling *et al.* (2006), and only the principal results will be reproduced here.

For a smooth pipe in the region of overlap, we expect a logarithmic variation of the velocity at sufficiently high Reynolds numbers. In inner variables it takes the form

$$U^+ = \frac{1}{\kappa} \ln y^+ + B \tag{1.4}$$

where $y^+ = yu_\tau/\nu$, $U^+ = U/u_\tau$, y is the distance from the wall, ν is the kinematic viscosity, and $u_\tau/\overline{U} = \sqrt{\lambda/8}$. In outer layer variables we have

$$U^+_{CL} - U^+ = -\frac{1}{\kappa} \ln \eta + B^* \tag{1.5}$$

where U_{CL} is the centreline velocity, $U^+_{CL} = U_{CL}/u_\tau$, and $\eta = y/R$. According to McKeon *et al.* (2004), $\kappa = 0.421 \pm 0.002$, $B = 5.60 \pm 0.08$, and $B^* = 1.2 \pm 0.1$. Furthermore, as reported by McKeon *et al.* and Zagarola & Smits (1998), the separation between the inner and outer scales must exceed a certain value before the expected logarithmic law appears. Zagarola & Smits (1998) identified a log law for Re higher than 400×10^3, but McKeon *et al.* modified this limit to 300×10^3 after applying more comprehensive Pitot probe corrections. Also, the log law was found to be valid for $600 \leqslant y^+ \leqslant 0.12R^+$. Here $R^+ = Ru_\tau/\nu$, and R is the pipe radius ($= D/2$).

With increasing Reynolds number and a fixed pipe diameter, the viscous length scale ν/u_τ decreases relative to D and may become comparable to the characteristic roughness height, k. At this point, roughness will start to play a role in determining the flow characteristics. If we assume, as argued by Townsend (1976), that roughness only affects the outer layer scaling by modulating the wall stress (that is, by changing u_τ), then the outer layer formulation is independent of roughness. In the overlap region,

$$U^+ = \frac{1}{\kappa} \ln y^+ + B - \Delta U^+ \tag{1.6}$$

where ΔU^+ is Hama's (1954) roughness function which is a function only of k^+. The Hama roughness function provides a convenient description of the behaviour in the transitional roughness regime.

It seems abundantly clear that different surface finishes have different transitional roughness behaviours, prompting further studies of rough-wall pipe flow. In such studies, it is important to cover the entire transitionally rough range from smooth to fully rough. This requirement dictates a sufficiently large Reynolds number range, something that can be achieved in the Princeton Superpipe facility used by Zagarola & Smits (1998) and Shockling *et al.* (2006). Here we report an investigation of commercial steel pipe roughness in the same facility for Reynolds numbers of 150×10^3 to 20×10^6. The investigation has important practical consequences in that commercial steel pipe is perhaps the most common type of surface finish (in terms of miles of pipe used) in engineering applications. No laboratory study of this particular surface has been performed since the early work of Bauer & Galavics (1936) and Galavics (1939), who investigated a commercially rough steel pipe with $k_{rms} = 130\,\mu\text{m}$ and $k_{rms}/D = 3.8 \times 10^{-4}$. The present surface with $k_{rms} = 5$ is probably more representative of a modern steel pipe, and thus our roughness to diameter ratio is also more realistic. This is supported by Sletfjerding, Gudmundsson & Sjøen (1998) who measured the roughness of an uncoated commercial steel pipe to be 2.36 μm (R_a) and 3.65 μm (R_q or k_{rms}). The pipe had an inner diameter of 150 mm. After coating the roughness dropped to 1.02 μm (R_a) and 1.32 μm (k_{rms}). Measurements reported by

Gersten *et al.* (2000) show $R_a = 8.5\,\mu$m for a commercial steel pipe. Diameter is not given.

2. Experiment

The pipe used in the experiments was 5 in. Schedule 40 welded steel pipe supplied by Lincoln Supply of Trenton, New Jersey. Welded steel pipe has a weld seam about 7–8 mm wide running along its entire length. Eight sections of pipe each of length 20 foot were obtained. The inner diameter of each length was measured at six different angles and at both ends. The inner diameter varied between 129.69 mm (5.106 in.) and 130.00 mm (5.118 in) with an average of 129.84 mm (5.112 in.). Near the weld, the pipe was slightly flattened so that the inside diameter decreased by a maximum amount of about 0.4 mm.

The test pipe was installed in the Princeton Superpipe facility that uses compressed air as the working fluid to generate a large Reynolds number range, in this case 150×10^3 to 20×10^6. The facility is described in more detail by Zagarola (1996) and Zagarola & Smits (1998).

The test pipe was constructed in eight separate sections, connected so that the inside surfaces were flush at each joint. The general design followed closely that used by Shockling *et al.* (2006). The steps at each joint in the assembled pipe were estimated to be less than about 50 μm, and they never occupied more than 10 % of the circumference. During assembly of the test pipe in the pressure vessel (described in detail by Zagarola 1996), a theodolite was used to align the sections along a target line. The maximum deviation from the target line at any point along the different segments was 1.5 mm, with an uncertainty of ± 0.5 mm. Note that a deviation of 1.5 mm at the middle of the longest segment (4.723 m long), yields a radius of curvature of about 1850 m, which is equal to $29\,000D$. Ito (1959) showed that the friction factor in curved pipes equals the value in straight pipes when

$$\Omega = Re_D \left(\frac{R}{R_0}\right)^2 \leqslant 0.034 \tag{2.1}$$

where R_0 is the radius of curvature. At a Reynolds number of 20×10^6 (the highest value attained in this experiment), $\Omega = 0.023$. Accordingly, the pipe was considered sufficiently straight to make curvature effects negligible.

A total of 21 streamwise pressure taps were used to measure the pressure gradient. The tap diameter was 0.79 mm and the streamwise spacing was 165.1 mm. The pressure taps were drilled from the outside of the pipe using very sharp drill-bits at high r.p.m. to minimize burr. The pressure taps were positioned approximately 120° relative to the weld seam.

A number of differential pressure transducers were used to cover the range of pressures encountered in this experiment. The lowest Reynolds number experiments ($< 250 \times 10^3$) were performed at atmospheric pressure using a 10 Torr MKS Baratron transducer with an uncertainty of ± 0.2 % of full scale. At higher Reynolds numbers, the vessel was pressurized, and Validyne DP-15 strain-gauge transducers were used with full-scale ranges of 0.2 p.s.i.d. (1380 Pa), 1.25 p.s.i.d. (8600 Pa), 5 p.s.i.d. (34 500 Pa) and 12 p.s.i.d. (83 000 Pa). The Validyne transducers are accurate to 0.5 % of full scale. By individually calibrating the transducers against sub-standards, the uncertainty was reduced to 0.25 % of full scale.

The atmospheric pressure was found using a mercury manometer, with an uncertainty of 35 Pa. The absolute pressure in the facility was measured with one of

two sensors. For pressures lower than 100 p.s.i.g. (0.7 MPa), an Omega transducer calibrated to an accuracy of ± 350 Pa was used. At higher pressures, a Heise pressure gauge was used with an uncertainty of 1 p.s.i.g. (7000 Pa). The air temperature was measured using a standard Chromel-Alumel thermocouple interfaced with an Omega DP-41-TC-AR indicator, accurate to ± 0.1 % (± 0.3 K at room temperature). A heat exchanger was used to keep the temperature in the pipe constant to within ± 0.6 K during an experiment.

2.1. *Velocity measurements*

The velocity profiles were taken approximately $200D$ downstream of the pipe inlet. A removable oval shaped plug, cut from an identical piece of pipe, was used to support the probe traverse assembly. The plug, measuring about 100 mm long and 50 mm wide, was hand-fitted to ensure a precise fit with the inside pipe surface. The plug was positioned approximately 120° relative to the weld seam, and 120° relative to the line of pressure taps. Two 0.40 mm static pressure taps were located on the plug surface and connected together to serve as the reference for the dynamic pressure. The mean velocity profile was measured by traversing a 0.40 mm diameter Pitot probe from the wall to the centreline of the pipe. The dynamic pressure was measured at 40 different wall distances, logarithmically spaced. The sampling time at each location was 90 s with a sampling frequency of 50 Hz. An Acurite linear encoder was used to determine the probe location with a resolution of ± 5 μm. It has been shown in previous experiments that the forward and reverse travel yielded repeatability within 25 μm (see Shockling *et al.* 2006).

To find the velocity from the Pitot probe measurements, we used the same corrections as those employed by Shockling *et al.* (2006), as originally proposed by Chue (1975), McKeon & Smits (2002) and McKeon *et al.* (2003). The uncertainty in the velocity ranges from 0.5 % to 2 % for the position closest to the wall, and reduces to 0.2 % to 0.5 % for the centreline velocity.

The mean velocity was found by integrating the velocity profile. For the points close to the wall a Spalding-type fit is used in the smooth regime, and a power-law fit is used when the flow is affected by wall roughness (see Shockling *et al.* 2006 for details). Since the Pitot probe corrections described above are only valid for a smooth wall, the points near the wall (for $y \leqslant 2d$ where d is Pitot tube diameter) were not included in the fit. In addition, for all the pressurized tests, that is, for $Re \geqslant 500\,000$, the points for $y^+ < 100$ are omitted in the calculation of the mean velocity to avoid the integration effects noted by Perry *et al.* (2001). In the transitionally rough regime, the difference between a Spalding fit and a power-law fit leads to differences in the friction factor that range from 0.6 % to 1.4 %. The corresponding uncertainty in Reynolds number is 0.3 % to 0.7 %.

The accurate determination of the traverse location adds very little uncertainty to the integrated profile, and is hence omitted.

2.2. *Friction factor measurements*

For incompressible fully developed pipe flow, the wall shear stress may be found from the pressure gradient according to the streamwise momentum equation, so that

$$\tau_w = -\frac{D}{4}\frac{\mathrm{d}p}{\mathrm{d}x}. \tag{2.2}$$

However, for a compressible flow, the acceleration term in the momentum equation is non-zero. By using the ideal gas law and assuming adiabatic flow, it is easily shown

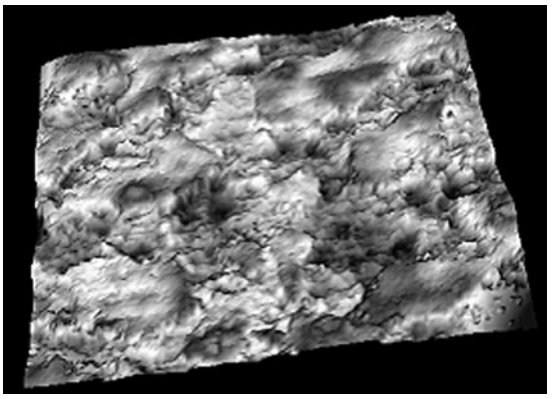

FIGURE 1. Surface scan of the pipe interior in a non-rust area. Sample size is 1.42×1.06 mm.

that

$$\tau_w = -\frac{D}{4}\left(1 - \frac{\rho}{\gamma p}U^2\right)\frac{\mathrm{d}p}{\mathrm{d}x}. \tag{2.3}$$

At velocities of $30\,\mathrm{m\,s^{-1}}$ the error in wall shear stress due to neglecting the acceleration term is about 0.7 %, which leads to an error of 0.35 % in the friction velocity. This inaccuracy propagates to the calculation of y^+ and u^+, but it does not affect the friction factor because the error appears in both the numerator and denominator of its definition (equation (1.2)).

The uncertainty in the friction factor originates primarily from the uncertainties in determining the pressure gradient and the dynamic pressure based on the average velocity. That is,

$$\frac{\Delta\lambda}{\lambda} = \sqrt{\left(\frac{\Delta(\mathrm{d}p/\mathrm{d}x)}{\mathrm{d}p/\mathrm{d}x}\right)^2 + \left(\frac{\Delta\left(\frac{1}{2}\rho\overline{U}^2\right)}{\frac{1}{2}\rho\overline{U}^2}\right)^2} \tag{2.4}$$

where Δ denotes the uncertainty level. The uncertainty in the pressure gradient is the main contributor. The surface roughness, and the possible imperfections in the pressure taps, introduced scatter in the wall pressure measurements which increased with Reynolds number. This is the main reason for the reported uncertainty level, which turned out to be larger than that of Shockling *et al.* (2006). The pressure gradient was found by a weighted least-squares fit to the 21 streamwise pressure measurements. The one-sigma confidence interval was used in the uncertainty calculations for the friction factor. The friction factor values agreed well with the expected values in the smooth flow regime, demonstrating that a two-sigma uncertainty interval is probably too conservative.

2.3. *Surface finish*

During the construction and installation of the test pipe, care was taken to preserve the surface finish as it was at the time of purchase, although an acetone wash was used to remove deposits of dirt and grease. Some spots of rust were found on the interior surface but they were accepted as an integral feature of a commercial steel pipe surface finish. The rust spots had a typical diameter of around 5 mm, and they covered less than about 1 % of the total surface area.

The surface geometry characteristics were measured using a Zygo non-interfering optical profiler. Typical topographical maps are shown in figure 1. The results for

	Commercial steel pipe	Honed aluminium pipe Shockling *et al.* (2006)
k_{rms} (μm)	5.0	2.5
k_{rms}/D	1:26000	1:52000
flatness/kurtosis	2.5	3.4
skewness	−0.19	0.31
λ_{HSC} (μm)	125–166	90
λ_{HSC}/k_{rms}	25–33	36

TABLE 1. Characteristic surface parameters.

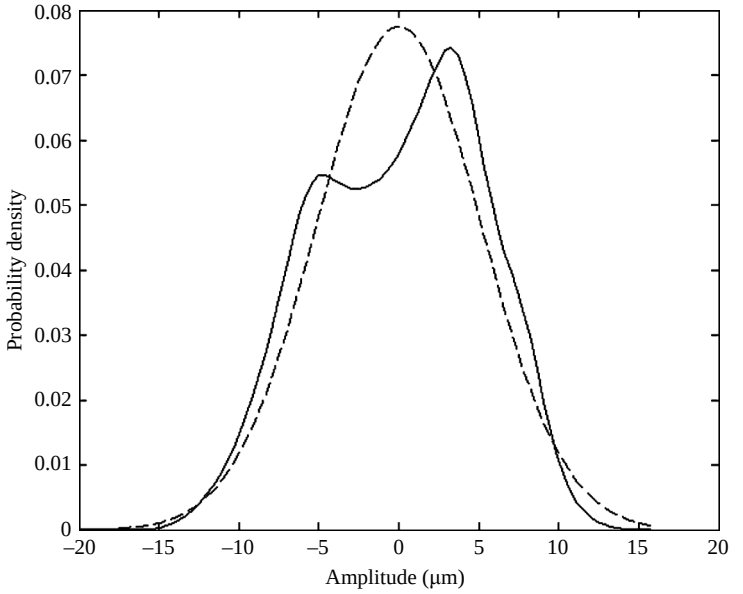

FIGURE 2. ——, Probability density function of commercial steel roughness; – – –, Gaussian distribution with the same standard deviation.

areas unaffected by rust are summarized in table 1, where a comparison with the honed surface studied by Shockling *et al.* (2006) is also given. The high spot-count wavelength, λ_{HSC}, is an estimate of the typical distance between the large roughness elements (in this case, the elements larger than k_{rms}). On the rust spots, the r.m.s. value was found to increase by approximately 0.5 to 1.0 μm, but the flatness and λ_{HSC} were unchanged.

The probability density function of the roughness height from measurements on six different samples is shown in figure 2. The distribution is clearly bimodal, indicating that two primary length scales are present. Inspection of the surface scans shows that the roughness is irregularly distributed, with relatively smooth regions separated by regions of more irregular, larger roughess elements. In contrast, the honed pipe studied by Shockling *et al.* (2006) had a unimodal PDF with a somewhat higher skewness and kurtosis (see table 1).

Re_D	λ	Re_D	λ
150×10^3	0.0167	2.0×10^6	0.0114
220×10^3	0.0155	2.8×10^6	0.0112
300×10^3	0.0146	3.9×10^6	0.0111
500×10^3	0.0134	5.5×10^6	0.0111
600×10^3	0.0132	7.5×10^6	0.0110
700×10^3	0.0127	10.5×10^6	0.0110
830×10^3	0.0122	14.8×10^6	0.0109
1.0×10^6	0.0121	20.0×10^6	0.0109
1.4×10^6	0.0117		

TABLE 2. Friction factor results.

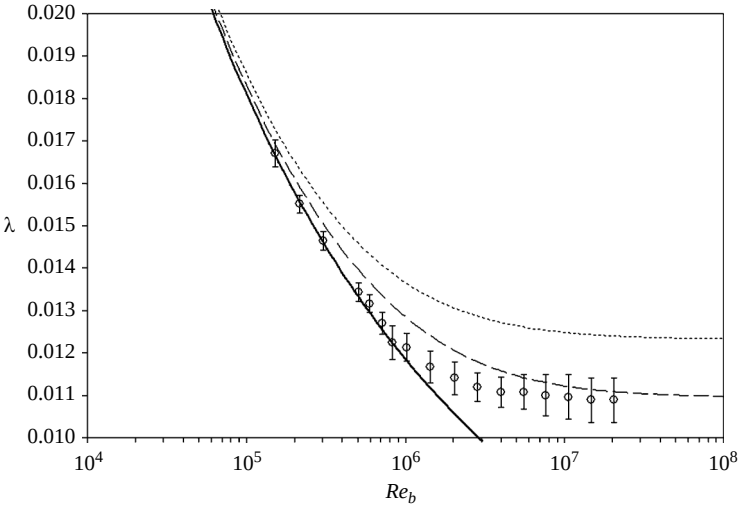

FIGURE 3. Friction factor results. ○, experiment; ——, equation (1.1); – – –, equation (1.3) with $k_s = 8\,\mu\text{m}$ ($= 1.6k_{rms}$); · · · · ·, equation (1.3) with $k_s = 15\,\mu\text{m}$ ($= 3.0k_{rms}$).

3. Results and discussion

3.1. *Friction factor*

The friction factor data listed in table 2 are shown in figure 3. The error bars indicate an uncertainty in friction factor of about $\pm 5\,\%$ at high Reynolds number (see § 2.2). The uncertainty in Reynolds number is insignificant when presented on a logarithmic scale.

For Reynolds numbers up to about $600 \times 10^3 \pm 100 \times 10^3$ the points collapse well on McKeon *et al.*'s (2004) smooth curve given by equation (1.1). The point of departure corresponds to $k_s^+ = 1.4 \pm 0.2$, which may be compared to a value of 3.5 for the honed aluminium pipe studied by Shockling *et al.* (2006). The friction factor becomes constant at a Reynolds number of $8.0 \times 10^6 \pm 2.0 \times 10^6$, indicating that the flow is fully rough, and that the pressure drop varies quadratically with the bulk velocity. The start of the fully rough regime corresponds to $k_s^+ = 18 \pm 4.0$. This is in the same range as reported by Shockling *et al.* (2006), but considerably lower than what is typically assumed. The equivalent sandgrain roughness is $1.6 \pm 0.5k_{rms}$, significantly lower than the more commonly accepted value of $(3 - 5k_{rms})$.

The transition to fully rough turbulent flow is abrupt, and it departs significantly from the Colebrook correlation. Furthermore, it does not exhibit the inflectional behaviour characteristic of Nikuradse's sandgrain roughness and the honed surface roughness studied by Shockling *et al.* (2006).

Based on the arguments of Colebrook & White (1937), the effects of roughness are first seen at a Reynolds number where the largest roughness elements begin to protrude outside the viscous sublayer. At this point, the flow between the large roughness elements is still dominated by viscous effects and more or less unaffected by roughness. As the Reynolds number increases, a larger portion of the viscous sublayer will be affected until finally the viscous sublayer vanishes, and the flow is fully rough. In this description of the transitional roughness response, the distance between the roughness elements must be an important parameter. For example, if the distance between the largest roughness elements is very small, then the small roughness elements will not play an important role since they will be shielded by the larger elements. Consequently the behaviour suggested by Colebrook & White not only depends on the roughness distribution, but also on the characteristic wavelengths. The present results indicate that the dependence on wavelength is not simple. For example, Nikuradse's sandgrain roughness displays a notable inflectional friction factor behaviour, and we would expect λ_{HSC}/k_{rms} to be about 2. This has been estimated by approximating the sandgrains by spheres, which gives a wavelength of the same order as the diameter. k_{rms} will be approximately $D/2$, resulting in the stated λ_{HSC}. For the honed surface, the inflectional behaviour is not so pronounced, and $\lambda_{HSC}/k_{rms} = 36$ for the honed surface. However, for the commercial steel surface there is no obvious inflection point in the friction factor curve, and $\lambda_{HSC}/k_{rms} = 25$–$33$, thereby running counter to the trend established by the other two surfaces.

Colebrook & White (1937) proposed that the largest roughness elements determine the point of departure from the smooth line, while the smallest roughness elements determine the point of collapse with the rough line. It may be inferred that a narrow size distribution would exhibit an inflectional behaviour, while a broader distribution would adhere more to the behaviour described by the Colebrook correlation. The natural rough steel pipe has a flatter roughness distribution than the previous honed aluminium pipe (that is, a lower kurtosis). Given that Nikuradse's sandgrain roughness distributions were tightly controlled, it is likely that the size distributions were even narrower than for the honed surface. The data appear to follow this trend, in that the size of the inflectional dip in the friction factor curves increases with decreasing kurtosis value.

Gioia & Chakraborty (2006) have recently developed a model for the shear that a turbulent eddy imparts to a rough surface. This model produces an inflectional friction factor–Reynolds number curve in the transitionally rough regime and links friction factor behaviour to the nature of the eddy interacting with the surface. However, the model is independent of roughness structure, and will not reproduce the commercial steel pipe measurements given here. G. Gioia (private communication) has recently extended this model to surfaces described by two distinct roughness types. This model will predict a monotonic friction factor curve with an abrupt transition from smooth to fully rough for the case where the height of one roughness is much smaller than the other (typically 1/1000), and where the areas covered by these roughnesses are comparable in size.

To see if this model can be applied to our commercial steel surface, we note first that the probability distribution of the roughness heights can be closely approximated by the sum of two normal distributions, each with a standard deviation of 3.2 μm,

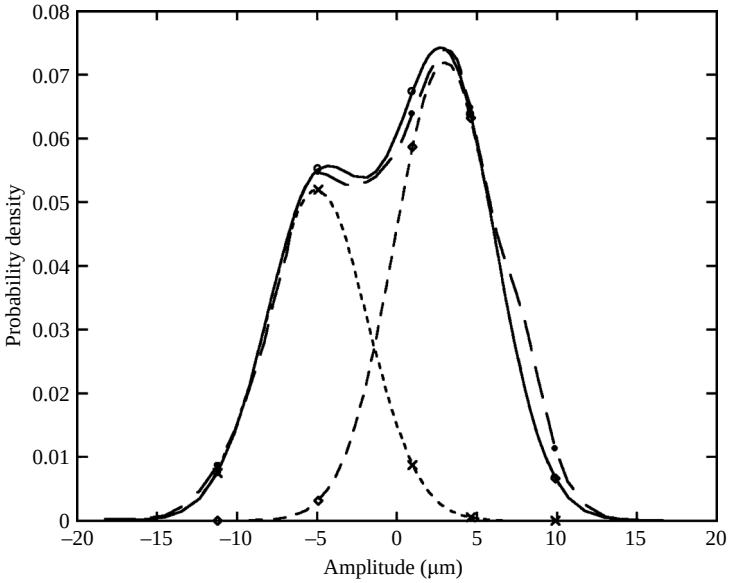

FIGURE 4. ——, Probability density function of commercial steel roughness as the sum of two Gaussian distributions with the same standard deviation. ——○——, experimental distribution; - - - × - - -, $0.052\exp(-((k+5)^2/20))$; - - - ○ - - -, $0.072\exp(-((k-3)^2/20))$; – – – ● – – –, sum of exponentials.

offset by a height of about 8 μm (see figure 4). The respective areas covered by the two distributions are in the ratio of their peak values, that is 58 % for the larger roughness, and 42 % for the smaller roughness, which falls within the scope of the extended Gioia model. However, whereas Gioia requires the two roughnesses to be very different in size, we see that in this experiment they have the same r.m.s. value, offset by a relatively large distance. The total span of the roughness elements covers about 30 μm, but it would be an exaggeration to describe one roughness as being very much smaller than the other. Commercial steel roughness is perhaps more accurately described as having three distinct length scales: the two standard deviations and the offset.

Along these lines, a simple model of the growing influence of roughness with increasing Reynolds number might be based on the relative area of roughness exposed by the thinning of the viscous sublayer. First, we choose the Reynolds number where roughness initially becomes important. We could choose the point where $5\nu/u_\tau \leqslant 30\,\mu\text{m}$ (taking the origin of the roughness to be at $-15\,\mu$m, as in figure 4). This Reynolds number corresponds closely to the point where the initial departure from the smooth curve is seen to occur in the experiment. Second, we assign a drag coefficient for the pressure drag of the roughness elements. Third, we assume that the total drag is given by the sum of the pressure and skin friction components, weighted by the areas they occupy (given by the running integral of the PDF of roughness heights). This model will generate an inflectional transitional roughness curve if the drag coefficient of the roughness elements is taken to be constant and equal to the friction factor in the fully rough regime (that is, about 0.0109). It will instead generate a monotonic behaviour similar to that seen in the experiment if the drag coefficient is allowed to vary from a value of about 0.013 to 0.0109 over the transitional roughness regime. This variation may be justified on the basis of low-Reynolds-number effects,

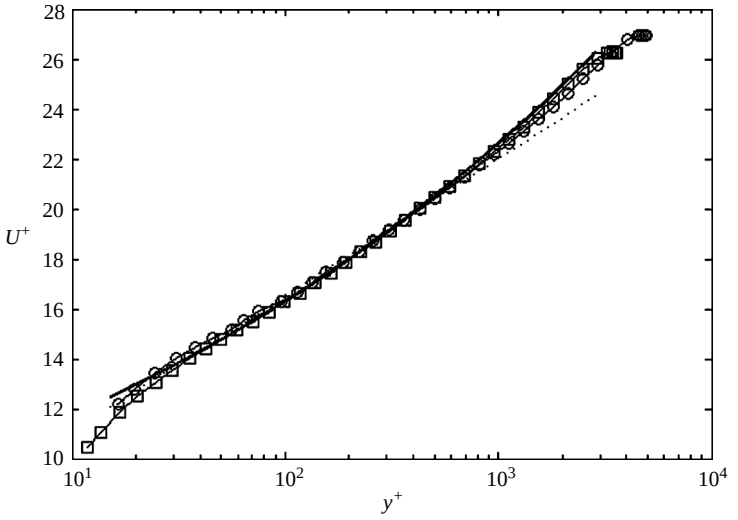

FIGURE 5. Velocity profiles, inner scaling, low Reynolds numbers. ——, equation (1.4); · · · · ·, power law from McKeon *et al.* (2004); □, Re_D 150×10^3; ○, 220×10^3.

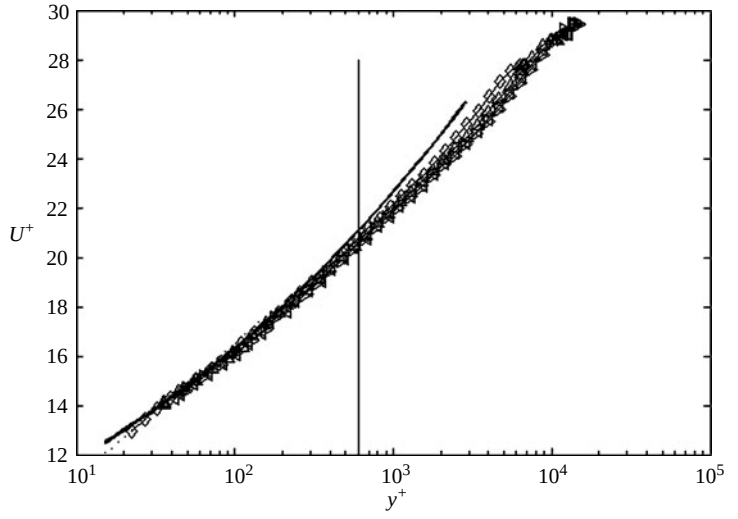

FIGURE 6. Velocity profiles, inner scaling, medium Reynolds numbers. ◇, Re_D 300×10^3; △, 500×10^3; ◁, 600×10^3; ▷, 700×10^3.

but the main point is that the drag mechanisms that govern the transitional roughness behaviour are undoubtedly subtle, and simple models are unlikely to give reliable predictive results without a good deal of additional information on the balance between friction and pressure drag in the near-wall region.

3.2. *Velocity profiles*

The velocity profiles for the two lowest Reynolds numbers are shown in figure 5. The velocity profiles collapse well with McKeon *et al.*'s (2004) power law, and at these low Reynolds numbers we do not expect to see a logarithmic region.

The velocity profiles for the other Reynolds numbers in the smooth flow regime (300×10^3–700×10^3) are shown in figure 6. The lower limit for the log law proposed

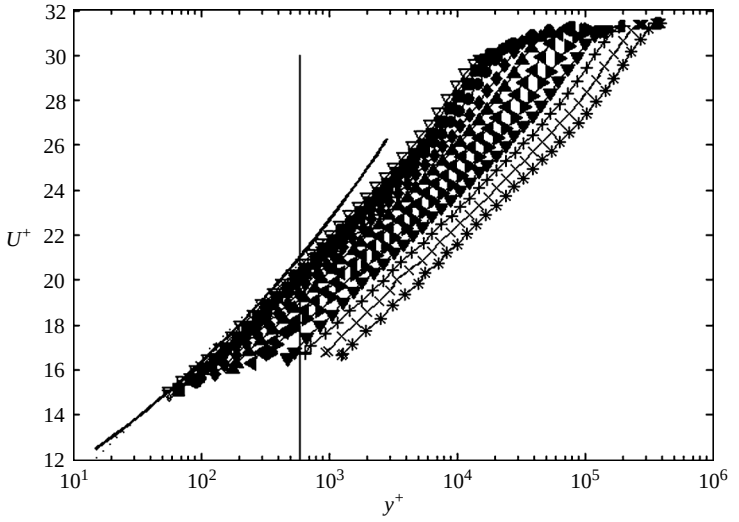

FIGURE 7. Velocity profiles, inner scaling, high Reynolds numbers. ▽, Re_D 830×10^3; ■, 1.0×10^6; ●, 1.4×10^6; ◆, 2.0×10^6; ▲, 2.8×10^6; ◄, 3.9×10^6; ►, 5.5×10^6; ▼, 7.5×10^6; +, 10.5×10^6; ×, 14.8×10^6; ⋆, 20.0×10^6.

by McKeon *et al.* (2004) is also shown, and the logarithmic region encompasses only a few points in the velocity profile.

The velocity profiles for the transitional and fully rough regimes are shown in figure 7. The downward shift in the profiles signals the onset of roughness, and with increasing Reynolds number the maximum value of U^+ becomes constant, indicating that the flow has become fully rough. The logarithmic region is clearly present for all Reynolds numbers in this range.

Figure 8 shows the velocity defect scaled by the friction velocity ($=(U_{CL}-U)/u_\tau$). The profiles collapse well in the overlap and outer layer regions for all data (i.e. smooth, transitionally rough, and fully rough wall). This lends support to Townsend's hypothesis of Reynolds number similarity, in that the mean relative motion in the fully turbulent region depends only on the wall stresses and pipe diameter (it is independent of the roughness, except in so far as a change in roughness changes the friction velocity). This agrees with the turbulence measurements of the high-Reynolds-number atmospheric boundary layer presented by Kunkel & Marusic (2006) and the turbulence data acquired in the previous honed rough pipe presented by Kunkel, Allen & Smits (2007).

3.3. *Roughness function*

The Hama roughness function ΔU^+ for the natural rough steel pipe is shown in figure 9. The function ΔU^+, as defined by equation (1.6), was found by minimizing the least-square error between the log law and the experimental data. It was assumed that $\kappa = 0.421$, as given by McKeon *et al.* (2004). The departure from the smooth behaviour occurs at $k_s^+ = 1.4 \pm 0.2$, as indicated earlier, but it is evident that the Colebrook function for the same k_s suggests that the effects of roughness start at a Reynolds number that is at least an order of magnitude lower. Also, for a given k_s value, the roughness function is greater than was found for the honed pipe, indicating that the downward shift of the velocity profile is relatively larger. This corresponds well with the differences in friction factor behaviour shown in figure 3.

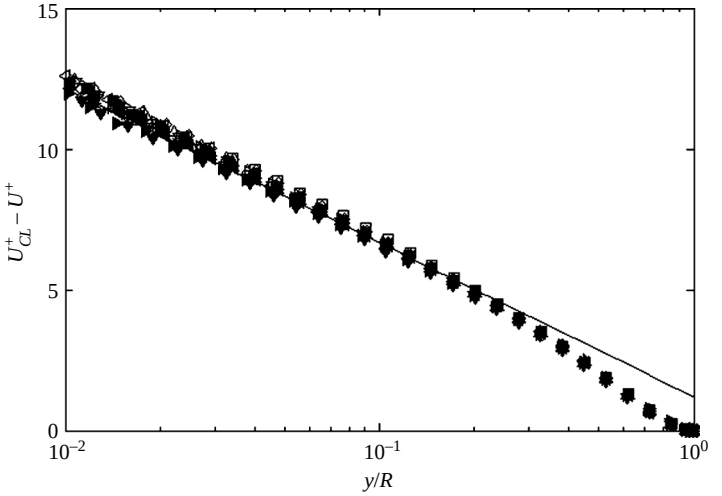

FIGURE 8. Velocity profiles, outer scaling. ——, equation (1.5); □, Re_D 150×10^3; ○, 220×10^3; ◇, Re_D 300×10^3; △, 500×10^3; ◁, 600×10^3; ▷, 700×10^3; ▽, Re_D 830×10^3; ■, 1.0×10^6; ●, 1.4×10^6; ◆, 2.0×10^6; ▲, 2.8×10^6; ◄, 3.9×10^6; ►, 5.5×10^6; ▼, 7.5×10^6; +, 10.5×10^6; ×, 14.8×10^6; ⋆, 20.0×10^6.

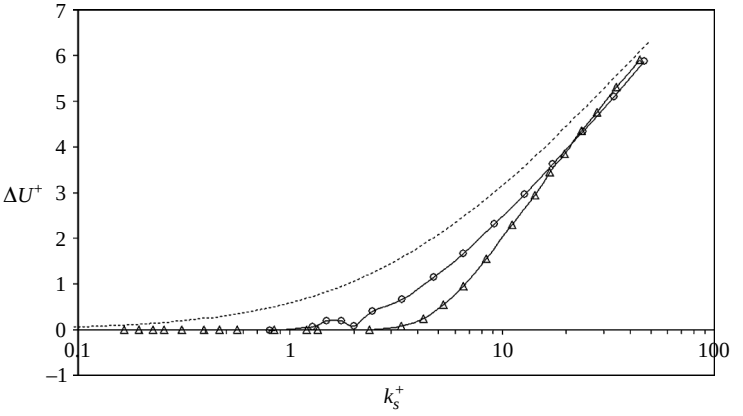

FIGURE 9. Hama roughness function. – – –, equation (1.3) with $k_s = 8\,\mu\text{m}$ ($= 1.6k_{rms}$); △, honed surface (Shockling *et al.* (2006)); ○, present results.

4. Friction factor diagram for commercial steel pipes

Our results suggest that the Moody diagram as currently constituted is not accurate for commercial steel pipe. Allen, Shockling & Smits (2005) have indicated how similarity arguments may be used to construct a complete friction factor diagram for a given surface using only a single friction factor data set, as long as the data cover the smooth to fully rough regime. The method requires as input the point of departure from the smooth regime, the point at which the fully rough regime begins, the equivalent sandgrain roughness, and a curve fit of the velocity profile in the wake region. Allen *et al.* (2005) gave results for the honed surface studied by Shockling *et al.* (2006). In figure 10, we use this method to suggest a new friction factor diagram for welded commercial steel pipe. Six curves corresponding to $k_s/D = 8.0 \times 10^{-6}$, 6.2×10^{-5}, 2.4×10^{-4}, 6.4×10^{-4}, 1.4×10^{-3}, and 2.7×10^{-3} are shown (the present

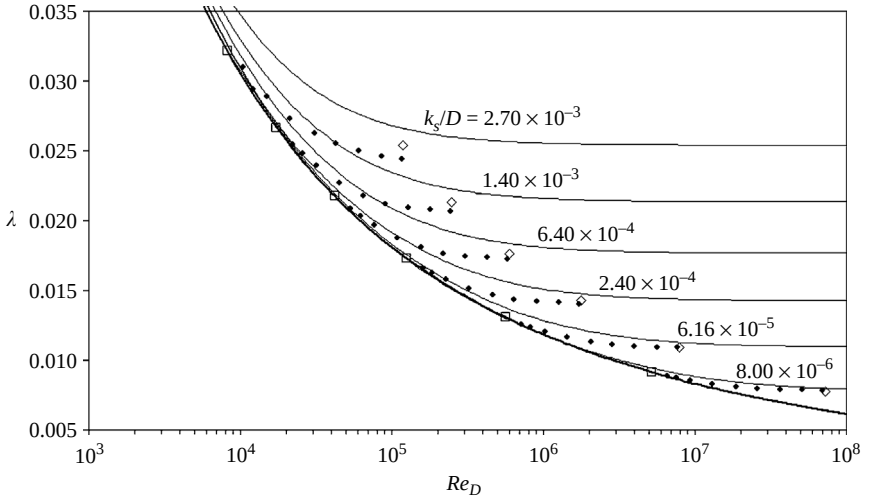

FIGURE 10. Proposed friction factor diagram for welded commercial steel pipe. ◆, Transitional roughness behaviour based on present measurements □, predicted point of departure from smooth line; ◇, predicted point of collapse with rough line; ——, Colebrook transitional roughness function (equation (1.3)).

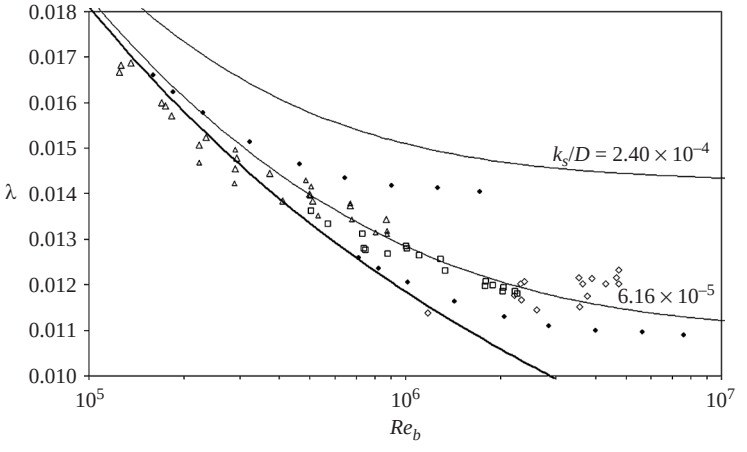

FIGURE 11. Measurements in a steel pipe by Bauer & Galavics (1936). □, $D = 450$ mm; ◇, $D = 350$ mm; △, $D = 250$ mm ◆, transitional roughness behaviour based on present measurements; ———; Colebrook transitional roughness function (equation (1.3)).

data had $k_s/D = 6.2 \times 10^{-5}$). As noted earlier, the transition region is considerably more abrupt than the Colebrook curve for the same equivalent sandgrain roughness would suggest. For increasing relative roughness, the end of the transition region (the rightmost ◆) deviates from the indicated point of collapse with the rough line (◇). The fitted wake function deviated slightly from the actual wake that was observed for $Re_D = 7.5 \times 10^6$, which is regarded as the last point in the transition region, and this error increases with lower Reynolds numbers.

The present results may be compared with the data obtained in steel pipes by Bauer & Galavics (1936) and Galavics (1939), as shown in figure 11. Steam at pressures ranging from about 3 to 6 bar was used as the working fluid, and the Reynolds

number was varied from 25×10^3 to 2.3×10^6. Three different pipes with diameters of 250, 350, and 450 mm were used. The manufacturing processes for the different pipes are not described in detail, and neither are their roughness characteristics, except that Bauer & Galavics (1936) report that for the 450 mm pipe $k_{rms} = 40\,\mu$m, so that $k_{rms}/D = 1/11000 = 8.9 \times 10^{-5}$, which is more than two times greater than the relative roughness of the pipe studied here. None of the measurements by Galavics & Bauer cover the complete transitional roughness region, so that definitive conclusions regarding the transitional roughness behaviour cannot be made, although some general observations are of interest.

The 250 mm measurements seem to depart from the smooth curve at around 300×10^3. Using $k_s^+ = 1.4$ as the departure point, $k_{rms}/D = 6.8 \times 10^{-5}$, and $k_{rms} = 17\,\mu$m. For the 450 mm series, the departure point cannot be determined with the same accuracy but it appears to be about the same as for the 250 mm series so that $k_{rms} \approx 30\,\mu$m, which agrees reasonably well with the value reported by Bauer & Galavics (1936). It appears, therefore, that the 250 mm and 450 mm results follow a similar transitional roughness behaviour to that observed in the present measurements, although the quality of commercial steel pipes seems to have improved considerably in the intervening 68 years (k_{rms}/D has dropped by a factor of 2). In contrast to the other two pipe sizes, the 350 mm results appear to belong to an inflectional curve, since the friction factor data display a minimum in the transitional roughness regime, although this may be a spurious observation since there is considerable scatter in the data.

5. Conclusions

Friction factor and mean velocity profiles were obtained in a commercial steel pipe ($k_{rms}/D = 1/26,000$) over a large Reynolds number range from 150×10^3 to 20×10^6. To the authors' knowledge, these are the first data for this commercially important surface finish to cover the entire range from smooth to fully rough.

The transitionally rough behaviour was found to be significantly different from that suggested by the Colebrook roughness function. In particular, the departure from the smooth curve is considerably more abrupt, and the fully rough regime is attained over a relatively small interval in Reynolds number. The curve appears to be monotonic, rather than inflectional as seen for sandgrain roughness (Nikuradse 1933) and honed surface roughness (Shockling *et al.* 2006). Since the Colebrook function was devised to describe 'natural' rough surfaces, these new data cast further doubt on its universality.

The probability distribution of the roughness heights can be closely approximated by the sum of two normal distributions, each with the same standard deviation of 3 μm, offset by a height of about 8 μm (the standard deviation of the combined distribution is 5 μm). The respective areas covered by the two distributions are about 58 % for the larger roughness, and 42 % for the smaller roughness. This observation suggests a stepped uncovering of the roughness elements as the Reynolds number increases. Two simple models discussed here help to give some insight into how this process may proceed, but fail to give predictive results.

We also note the equivalent sandgrain roughness was found to be about $1.6k_{rms}$, instead of the commonly accepted value of 3–5 k_{rms}. For the fully rough regime, and indeed for most of the transitional regime, this gives a friction factor about 13 % lower than that given by the Moody diagram using $k_s = 3.2k_{rms}$.

Finally, the mean velocity profiles support Townsend's similarity hypothesis for flow over rough surfaces. See also Flack, Schultz & Shapiro (2005) and Shockling *et al.* (2006).

Financial support was received from ONR under Grant N00014-03-1-0320 and NSF under Grant CTS-0306691. L. I. L. was supported by a graduate research fellowship from the Norwegian Research Council, and G. J. K. was supported in part by Princeton University through a Council on Science and Technology Fellowship. Special thanks are due to Bob Bogart for contributing his technical skills to the design and installation of the pipe.

REFERENCES

Allen, J. J., Shockling, M. A. & Smits, A. J. 2005 Evaluation of a universal transition resistance diagram for pipes with honed surfaces. *Phys. Fluids* **17**, 121702.

Blasius, H. 1913 Das Ahnlichkeitsgesetz bei Reibungvorgangen in Flussigkeiten. *Forschg. Arb. Ing.* **135**.

Bradshaw, P. 2000 A note on 'critical roughness height' and 'transitional roughness'. *Phys. Fluids* **12**, 1611–1614.

Bauer, B. & Galavics, F. 1936 Untersuchungen über die Rohrreibung bei Heiβwasserfernleitungen. *Archiv Waermewirtschaft* **17** (5), 125–126.

Chue, S. H. 1975 Pressue probes for fluid measurement. *Prog. Aerospace Sci.* **16** (2), 1–40.

Colebrook, C. F. 1939 Turbulent flow in pipes, with particular reference to the transitional region between smooth and rough wall laws. *J. Inst. Civil Engrs* **11**, 133–156.

Colebrook, C. F. & White, C. M. 1937 Experiments with fluid friction in roughened pipes. *Proc. R. Lond. Soc.* A **161**, 367–378.

Flack, K. A., Schultz, M. P. & Shapiro, T. A. 2005 Experimental support for Townsend's Reynolds number similarity hypothesis on rough walls. *Phys. Fluids* **17**, 035102.

Galavics, F. 1939 Die Methode der Rauhigkeitscharakteristik zur Ermittlung der Rohrreibung in geraden Stahlrohr-Fernleitungen. *Schweizer Archiv* **5** (12), 337–354.

Gersten, K., Papenfuss, H.-D., Kurschat, T., Genillon, P., Fernandez Perez, F. & Revell, N. 2000 New transmission-factor formula proposed for gas pipelines. *Oil & Gas J.* **98** (7), 58–62.

Gioia, G. & Chakraborty, P. 2006 Turbulent friction in rough pipes and the energy spectrum of the phenomenological theory. *Phys. Rev. Lett.* **96**, 044502.

Hama, F. R. 1954 Boundary-layer characteristics for smooth and rough surfaces. *Trans SNAME* **62**, 333–358.

Ito, H. 1959 Friction factors for turbulent flow in curved pipes. *Trans. ASME: J. Basic Engng* **6**, 123.

Kunkel, G. J. & Marusic, I. 2006 Study of the near-wall-turbulent region of the high-Reynolds-number boundary layer using an atmospheric flow. *J. Fluid Mech.* **548**, 375–402.

Kunkel, G. J., Allen, J. J. & Smits, A. J. 2007 Further support for Townsend's Reynolds number similarity hypothesis in high Reynolds number rough-wall pipe flow. *Phys. Fluids* **19**, 055109.

Langelandsvik, L. I., Postvoll, W., Svendsen, P., Øverli, J. M. & Ytrehus, T. 2005 An evaluation of the friction factor formula based on operational data. *Proc. 2005 PSIG Conference, San Antonio, Texas.*

McKeon, B. J. & Smits, A. J. 2002 Static pressure correction in high Reynolds number fully developed turbulent pipe flow. *Meas. Sci. Tech.* **13**, 1608–1614.

McKeon, B. J., Li, J., Jiang, W., Morrison, J. F. & Smits, A. J. 2003 Pitot probe corrections in fully-developed turbulent pipe flow. *Meas. Sci. Tech.* **14**, 1449–1458.

McKeon, B. J., Li, J., Jiang, W., Morrison, J. F. & Smits, A. J. 2004 Further observations on the mean velocity distribution in fully developed pipe flow. *J. Fluid Mech.* **501**, 135–147.

McKeon, B. J, Zagarola, M. V. & Smits, A. J. 2005 A new friction factor relationship for fully developed pipe flow. *J. Fluid Mech.* **538**, 429–443.

Moody, L. F. 1944 Friction factors for pipe flow. *Trans. ASME* **66**, 671–684.

NIKURADSE, J. 1933 Laws of flow in rough pipes. *VDI Forschungsheft* **361**. Also *NACA TM* **1292**, 1950.

PERRY, A. E., HAFEZ, S. & CHONG, M. S. 2001 A possible reinterpretation of the Princeton superpipe data. *J. Fluid Mech.* **439**, 395–401.

PRANDTL, L. 1935 The mechanics of viscous fluids. In *Aerodynamic Theory III* (ed. W. F. Durand), p. 142; also Collected Works II, pp. 819–845.

SHOCKLING, M. A., ALLEN, J. J., SMITS, A. J. 2006 Roughness effects in turbulent pipe flow. *J. Fluid Mech.* **564**, 267–285.

SLETFJERDING, E., GUDMUNDSSON, J. S. & SJØEN, K. 1998 Flow experiments with high pressure natural gas in coated and plain pipes. *Proceedings of the 1998 PSIG Conference* Denver, Colorado.

TOWNSEND, A. A. 1976 The Structure of Turbulent Shear Flow. *Cambridge University Press.*

ZAGAROLA, M. V. 1996 Mean-flow scaling of turbulent pipe flow. Doctoral Dissertation, Princeton University.

ZAGAROLA, M. V. & SMITS, A. J. 1998 Mean-flow scaling of turbulent pipe flow. *J. Fluid Mech.* **373**, 33–79.